Ordering by Collapse: Formation of Bilayer and Trilayer Crystals by Folding Langmuir Monolayers

David Vaknin,*,† Wei Bu,† Sushil K. Satija,‡ and Alex Travesset†

Ames Laboratory and Department of Physics and Astronomy, Iowa State University, Ames, Iowa 50011, and NIST Center for Neutron Research, National Institute of Standards and Technology, Gaithersburg, Maryland 20899-8562

Received September 12, 2006. In Final Form: November 20, 2006

Neutron and synchrotron X-ray studies of arachidic-acid monolayers compressed to the collapse region, beyond their densely packed molecular area, reveal that the resulting structures exhibit a surprising degree of reproducibility and of order. The structure of the collapsed monolayers differs for films that are spread on pure water or on $CaCl_2$ solutions. On pure water, the collapsed monolayer forms a stable crystalline trilayer structure, with acyl-chain in-plane packing practically identical to the three-dimensional (3D) crystal structure of fatty acids. For monolayers spread on Ca^{2+} solutions, the collapsed film consists of a bi- and trilayer mixture with a ratio that changes by the collapse protocol. Our analysis suggests that the bilayer structure is inverted, i.e., with the hydrophobic tails in contact with the water surface and the calcium ions bridging the polar heads. The inverted bilayer structure possesses a well-ordered crystalline slab of calcium oxalate monohydrate intercalated between two acyl chains. We provide theoretical arguments rationalizing that the observed structures have lower free energies compared with other possible structures and contend that the collapsed structures may, under certain circumstances, form spontaneously.

I. Introduction

Under controlled compression and temperature conditions, insoluble monolayers at gas/water interfaces (Langmuir monolayers) exhibit a plethora of phases, including quasi-two-dimensional (2D) gaseous, liquid, and a few solid phases.[1−5] The structure and properties of the saturated fatty acids, for example, have been thoroughly studied as model systems of Langmuir monolayers to unravel these phases.[4−8] As the monolayer is compressed and the surface pressure (π) is increased beyond a critical value, usually occurring at the minimal closely packed molecular area (i.e., the average cross section of the molecule, A_0), the monolayer fractures and/or folds, forming multilayers[9−11] in a process referred to as *collapse*. *Spontaneous collapse*, where the breakage and/or folding occurs at molecular areas $A \gtrsim A_0$ and the monolayer coexists with its bulk phase, has also been reported.[10,12−15] These processes are the primary cause for surface-pressure relaxation of a monolayer that is kept at a constant surface area or for the reduction in surface area when the monolayer is maintained at a constant surface pressure.[1] Whether the collapse is *spontaneous* or *induced*, the products formed in these processes can be either soluble or insoluble aggregates with morphologies that primarily depend on the nature of the molecules constituting the monolayer and the subphase conditions. It was also reported that the compression rate is an important factor that influences the collapse.[16] Although processes leading to collapse are generally irreversible, certain mixed monolayers, in particular, those including surface proteins, can be compressed beyond the initial collapse point (ICP) and expanded to form a monolayer, reversibly. Reversible collapse in mixed monolayers consisting of lung surfactants has been extensively studied in recent years to unravel the mechanics of surface tension regulation in the lungs.[17−20] Other investigations of collapsed monolayers are, in part, motivated by the notion that the underlying principles governing collapse are relevant to understanding biological processes such as the response of membranes to stress, membrane fusion and fission, and other cell membrane processes.[21,22] Furthermore, understanding how ions in solution, particularly calcium, affect the collapse is relevant to membrane fusion processes.[23]

Various mechanisms for monolayer collapse and the resulting reorganization of the film have been proposed. Micrographs of collapsed 2-hydroxytetracosanoic acid films, after being transferred to solid support, were used to propose that collapse proceeds by the formation of double-layer platelets (bonded at their headgroups). The platelets are initially formed at the weakened boundaries emanating from the monolayer toward the vacuum and grow in size until they break and stack on the monolayer to form an inhomogeneous trilayer film.[9] Imaging with light

* To whom correspondence should be addressed.
† Iowa State University.
‡ National Institute of Standards and Technology.

(1) Gaines, G. *Insoluble Monolayers at the Liquid-Gas Interface*; Interscience: New York, 1966.
(2) Lundqvist, M. *Prog. Chem. Fats Other Lipids* **1978**, *16*, 101.
(3) MacRitchie, F. *Chemistry at Interfaces*; Academic Press Inc.: San Diego, 1990.
(4) Kjaer, K.; Als-Nielsen, J.; Helm, C.; Tippman-Krayer, P.; Möhwald, H. *J. Phys. Chem.* **1989**, *93*, 3200.
(5) Bibo, A. M.; Knobler, C. M.; Peterson, I. R. *J. Phys. Chem.* **1991**, *95*, 5591.
(6) Kenn, R. M.; Boehm, C.; Bibo, A. M. *J. Phys. Chem.* **1991**, *95*, 2092.
(7) Durbin, M. K.; Richter, A. G.; Yu, C.-J.; Kmetko, J. M.; Bai, J. M.; Dutta, P. *Phys. Rev. E* **1998**, *58*, 7686.
(8) Kaganer, V.; Möhwald, H.; Dutta, P. *Rev. Mod. Phys.* **1999**, *71*, 779.
(9) Ries, H. E., Jr. *Nature* **1979**, *281*, 287.
(10) Smith, R. D.; Berg, J. C. *J. Colloid Interface Sci.* **1980**, *74*, 273.
(11) McFate, C.; Ward, D.; Olmsted, J. *Langmuir* **1993**, *9*, 1036.
(12) Rabinovitch, W.; Robertson, R. F.; Mason, S. G. *Can. J. Chem.* **1960**, *38*, 1881.
(13) Neuman, R. D. *J. Colloid Interface Sci.* **1976**, *56*, 505.
(14) Meine, K.; Weidemann, G.; Vollhardt, D.; Brezesinski, G.; Kondrashkina, E. A. *Langmuir* **1997**, *13*, 6577 and references therein.
(15) Hatta, E. *Langmuir* **2004**, *20*, 4059.
(16) Ybert, C.; Lu, W.; Moller, G.; Knobler, C. *J. Phys. Chem. B* **2002**, *106*, 2004.
(17) Wang, Z. D.; Hall, S. B.; Notter, R. H. *J. Lipid Res.* **1995**, *36*, 1283.
(18) Robertson, B.; Halliday, H. L. *Biochim. Biophys. Acta* **1998**, *1408*, 346.
(19) Lipp, M. M.; Lee, K. Y. C.; Takamoto, D. Y.; Zasadzinski, J. A.; Waring, A. J. *Phys. Rev. Lett.* **1998**, *81*, 1650.
(20) Warriner, H. E.; Ding, J.; Waring, A. J.; Zasadzinski, J. A. *Biophys. J.* **2002**, *82*, 835 and references therein.
(21) Epand, R. M.; Vogel, H. J. *Biochim. Biophys. Acta* **1999**, *1462*, 11.
(22) Chernomordik, L. V.; Kozlov, M. M. *Annu. Rev. Biochem.* **2003**, *72*, 25.
(23) Vogel S. S.; Zimmerberg, J. *Proc. Natl. Acad. Sci. U.S.A.* **1992**, *89*, 4749.

10.1021/la062672u CCC: $37.00 © 2007 American Chemical Society
Published on Web 01/04/2007

microscopy and topographic micrographs of transferred collapsed films of the same molecules suggest that the collapse process depends on surface pressure and also on the rate of compression. For low surface pressures, multilayer islands are formed by *spontaneous collapse*, whereas platelet folding occurrs by *induced collapse*. At low compression rates, giant platelets that protrude into the subphase (i.e., exposing the headgroups of the bilayer to water) are formed in a reversible process that, by expansion, respread as a monolayer.[16] The collapse of 10,12-pentacosaiyonic acid studied by X-ray reflectivity and atomic force microscopy (AFM) shows that the collapse proceeds by multilayer formation, with no evidence of folding or platelet formation.[24] Phase contrast microscopy (PCM) studies of tetracosanoic acid monolayers suggest a surface-roughening collapse and subsequent anisotropic cracking in the form of curved filaments.[15] More involved folding mechanisms of amphiphile mixtures with different spontaneous curvatures have also been proposed.[25]

The effect of ions in solution on the collapse of fatty acids has been investigated mostly by transferring the monolayer to a solid support[13,15,26] but has not been adequately characterized *in situ*. *In situ* investigations of monolayer collapse on multivalent ion solutions are particularly interesting, as it is well-known that, before collapse, multivalent ions form a firm layer (Stern layer) of counterions at the carboxylic headgroups.[4,27] Rather surprisingly, in some circumstances, under suitable pH conditions and long relaxation times, diffraction studies have found a plethora of Bragg peaks that have been interpreted as the ions forming a 2D superlattice crystalline structure contiguous to the carboxylic headgroup, in direct contact with the water.[28,29] We point out, however, that the formation of crystalline multilayers by spontaneous collapse was reported for fatty acid monolayers spread on calcium solutions.[13] Furthermore, a recent PCM study of a monolayer spread on Cd^{2+} solutions revealed the formation of isolated domains in the absence of surface pressure, attributed to a spontaneous collapse of the monolayer.[15] In view of these findings, it is plausible that spontaneous collapse may give rise to Bragg peaks, and reflectivity studies are, therefore, crucial to determine whether those peaks correspond to structures within the aqueous solution or within a collapsed film.

The exact nature of collapsed monolayers on solutions of divalent ions at the gas/water interface remains an open question. We have, therefore, undertaken the present surface neutron and synchrotron X-ray studies to systematically determine the structures of monolayers undergoing induced collapse. In this manuscript, we present investigations of arachidic acid (AA) before and after collapse and spread on pure and Ca^{2+} water solutions. To characterize the collapsed films, we measured the $\pi-A$ isotherms and conducted neutron and synchrotron X-ray reflectivity and grazing incidence X-ray diffraction (GIXD) to determine the structures of the films. When starting this project, we did not expect the resulting collapsed films to exhibit the surprising degree of order that we observed experimentally.

II. Experimental Details

Monolayers of protonated and deuterated arachidic acid were prepared at gas/water interfaces in a thermostatic, solid Teflon Langmuir trough and spread from 3:1 chloroform/methanol solutions (deuterated arachidic acid, $CD_3(CD_2)_{18}COOH$, catalog no. DLM-1233-1, was purchased from Cambridge Isotope Laboratories, Woburn, MA). $CaCl_2 \cdot 2H_2O$ was purchased from Sigma Inc. and used as provided. Ultrapure water (Millipore, Milli-Q, and NAN-Opure, Barnstead; resistivity, 18.1 MΩ/cm) was used for all subphase preparations. D_2O (D at 99.8%) for neutron reflectivity experiments was purchased from Cambridge Isotope Laboratories, Woburn, MA (catalog no. DLM-2259-1). Pure light and heavy water and salt solutions were used without any buffer to adjust the pH (pH ∼ 6.5). Compression of the monolayer was started 10−15 min after spreading the monolayer to allow for solvent evaporation. The monolayer was then compressed to a desired surface pressure at compression rates of 0.29−0.58 $Å^2$/min, and the surface pressure was recorded with a microbalance using a filter paper Wilhelmy plate. We distinguish two protocols for the collapse: (1) the film is compressed at the compression rate specified above to the collapse regime and (2) the film is compressed to form a densely packed monolayer (before collapse) and, after a waiting period of 6−24 h (after conducting experiments at this regime), the film is further compressed to the collapse regime. To minimize radiation damage due to the formation of radicals and ions and to reduce background scattering from air, the films were kept under a water-saturated helium environment during the synchrotron X-ray experiments. The trough was mounted on a motorized stage that can translate the surface laterally with respect to the incident beam, enabling the illumination of different parts of the monolayer to monitor radiation damage.

Neutron reflectivity measurements were performed on the NG7 horizontal reflectometer at the NIST (National Institute of Standards and Technology) Center for Neutron Research (NCNR). The neutron scattering intensity was collected along the specular reflection direction and plotted as a function of the *z*-directional scattering wave vector, $Q_z = (4\pi/\lambda) \sin \alpha$, where the neutron wavelength is $\lambda = 4.75$ Å and α is the incident angle to the substrate. The X-ray studies at gas/water interfaces were conducted on the Ames Laboratory liquid surface diffractometer at the Advanced Photon Source (APS), beamline 6ID-B (described elsewhere[30]). The highly monochromatic beam (16.2 keV; $\lambda = 0.765334$ Å) selected by a downstream silicon double-crystal monochromator is deflected onto the liquid surface to a desired angle of incidence with respect to the liquid surface by a second monochromator [Ge(2,2,0)] located on the diffractometer.[31]

Neutron and X-ray reflectivity (NR and XR, respectively) and grazing incident X-ray diffraction (GIXD) techniques are commonly used to characterize the monolayer structure.[30,32−35] NR and XR experiments yield the scattering length density (SLD) and the electron density (ED) profiles across the interface and can be related to the molecular arrangements in the film. The density profiles across the interface are extracted by refining a slab model that best fits the measured reflectivity by the nonlinear least-squares fit (NLSF) method. The SLD and ED profile $\rho(z)$ is constructed by a sum of error functions:

$$\rho(z) = \frac{1}{2}\sum_{i=1}^{N+1} \mathrm{erfc}\left(\frac{z - z_i}{\sqrt{2}\sigma_i}\right)(\rho_i - \rho_{i+1}) + \frac{\rho_1}{2} \qquad (1)$$

where $N + 1$ is the number of interfaces, $\rho_i - \rho_{i+1}$, z_i, and σ_i are the change in the ED, the position, and the roughness of *i*th interface, respectively, ρ_1 is the SLD or ED of the subphase, and $\rho_{N+2} \approx 0$ is the density of the gas phase. The variable parameters are ρ_i, z_i (the

(24) Gourier, C.; Knobler, C.; Daillant, J.; Chatenay, D. *Langmuir* **2002**, *18*, 9434.
(25) Diamant, H.; Witten, T.; Ege, C.; Gopal, A.; Lee, K. Y. C. *Phys. Rev. E* **2001**, *63*, 61602.
(26) Kundu, S.; Datta, A.; Hazra, S. *Langmuir* **2005**, *21*, 5894.
(27) Shih, M. C.; Bohanon, T. M.; Mikrut, J. M.; Szchack, P.; Dutta, P. *J. Chem. Phys.* **1991**, *96*, 1556.
(28) Leveiller, F.; Jacquemain, D.; Lahav, M.; Leiserowitz, L.; Deutch, M.; Kjaer, K.; Als-Nielsen, J. *Science* **1991**, *252*, 1532.
(29) Kmetko, J.; Datta, A.; Evmenenko, G.; Durbin, M. K.; Richter, A. G.; Dutta, P. *Langmuir* **2001**, *17*, 4697.
(30) Vaknin, D. In *Methods in Materials Research*; Kaufmann, E. N., et al., Eds.; Wiley: New York, 2001; p 10d.2.1.
(31) Als-Nielsen, J.; Pershan, P. S. *Nucl. Instrum. Methods Phys. Res.* **1983**, *208*, 545.
(32) Als-Nielsen, J.; Kjaer, K. In *Phase Transitions in Soft Condensed Matter*; Riste, T., Sherrington, D., Eds.; Plenum: New York, 1989.
(33) Penfold, J.; Thomas, R. K. *J. Phys.: Condens. Matter* **1990**, *2*, 1369.
(34) Vaknin, D.; Kjaer, K.; Als-Nielsen, J.; Lösche, M. *Biophys. J.* **1991**, *59*, 1325.
(35) Vaknin, D.; Kjaer, K.; Als-Nielsen, J.; Lösche, M. *Makromol. Chem.* **1991**, *46*, 383.

thicknesses of the slabs associated with different parts of the molecules are denoted as $d_i \equiv |z_i - z_{i-1}|$), and the roughness σ_i. The continuous SLD or ED is sliced into a histogram (several hundred slices) to compute the reflectivity by the recursive dynamical method.[36,37]

From the numerous attempted models for analyzing the data, the most consistent and satisfactory ones were those for which the collapsed films consisted of mono-, bi-, and trilayer mixtures. The model density profile for the monolayer is well-established.[4] It consists of two uniform slabs of distinct ED/SLDs: one associated with the headgroup in contact with the subphase and the other associated with the acyl chains in contact with the gas interface. The bilayer (or inverted bilayer) structure is a novel configuration, consisting of an SLD/ED that corresponds to two AA molecules attached at their headgroups and stretched to form a dimer, which, although hydrophobic at both ends, resides at water, as shown in Figure 1. The trilayer structure consists of a bilayer on top of a monolayer, as shown schematically in Figure 1. The reflectivity from the inhomogeneous films is assumed to consist of incoherent scattering from the three components as follows:

$$R(Q_z) = \alpha R_{\mathrm{mono}}(Q_z) + \beta R_{\mathrm{bi}}(Q_z) + \gamma R_{\mathrm{tri}}(Q_z) \qquad (2)$$

where $\alpha + \beta + \gamma = 1$. In all cases, we compressed the film to the nominal molecular area in the range $A_0/3 \leq A \leq A_0/2$. Figure 1 shows the calculated X-ray and neutron reflectivities (A and B) of possible EDs and SLDs (C and D) for the mono-, bi-, and trilayers. The calculated reflectivities were used to identify the main features in the measured reflectivities to determine qualitatively their compositions.

GIXD measurements were conducted to determine the lateral organization in the film. In these experiments, the angle of the incident beam with respect to the surface, α, is fixed below the critical angle ($\alpha_c = \lambda(\rho_s r_0/\pi)^{1/2}$; $r_0 = 2.82 \times 10^{-13}$ cm, where ρ_s is the subphase ED) for total reflection, while the diffracted beam is detected at a finite azimuthal in-plane angle, 2Θ, and out-of-plane angle, β (the angle of the reflected beam with respect to the surface). Rod scans along the surface normal at the 2D Bragg reflections enable the determination of the average ordered chain length and tilt angle with respect to the surface normal. The intensity along the rod scan of a 2D Bragg reflection is analyzed in the framework of the distorted wave Born approximation (DWBA):

$$I(Q_{xy}, Q_z) \propto |t(k_{z,i})|^2 |F(Q_z)|^2 |t(k_{z,f})|^2 \qquad (3)$$

where $t(k_{z,i})$ and $t(k_{z,f})$ ($k_{z,i} = k_0 \sin \alpha$; $k_{z,f} = k_0 \sin \beta$) are the Fresnel transmission functions, which give rise to enhancements around the incoming (α) and outgoing (β) critical angles. The in-plane momentum transfer is given by $Q_{xy} = (Q_x^2 + Q_y^2)^{1/2}$.[38] In modeling, the length and the tilt angle are varied, and the intensities are adjusted for two tilt directions: toward nearest-neighbors (NN) and toward next NN (NNN).[4,32,39] The form factor for the tails is given by

$$F(Q_z') = \sin(Q_z' l/2)/(Q_z' l/2) \qquad (4)$$

where Q_z' is defined along the long axis of the chain and l is the chain length.

III. Experimental Results

A. π−*A* Isotherms. Figure 2 shows surface pressure versus molecular area (π−A) isotherms of arachidic acid spread on water and on a 10^{-3} M $CaCl_2$ solution as indicated. The isotherm of AA is typical of fatty acids.[2] Before collapse, at molecular areas slightly larger than the cross section of acyl chains ($A_0 \approx 20$ Å^2), the isotherm has a distinct transition at surface pressure,

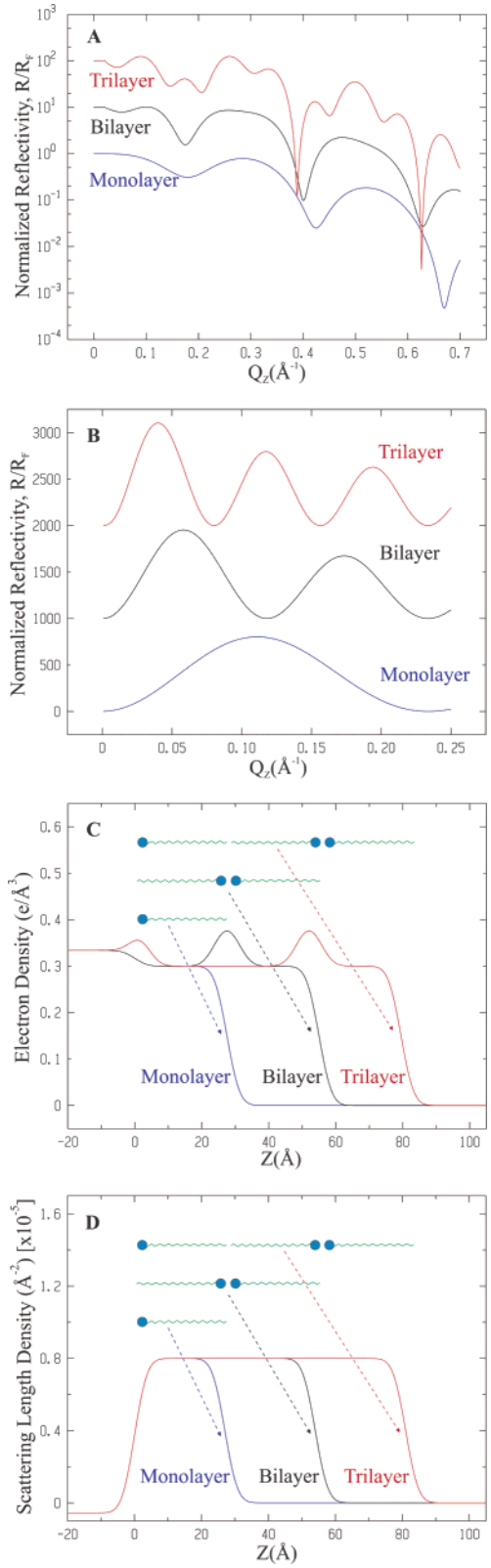

Figure 1. (A) Calculated XRs and (B) NRs normalized to the reflectivities of the subphases (R_F) for mono-, bi-, and trilayers (XRs and NRs are shifted for clarity). (C) Corresponding EDs and (D) SLDs used to calculate the reflectivities. The calculations of the NRs were performed for deuterated AA uniformly spread on H_2O (the SLDs of the headgroups for the neutrons are practically the same as those of the deuterated chains).

(36) Born, M.; Wolf, E. *Principles of Optics*; MacMillan: New York, 1959.
(37) Parratt, L. G. *Phys. Rev.* **1954**, *59*, 359.
(38) The coordinate system used in this manuscript is such that Q_z is normal to the liquid surface, Q_x is parallel to the horizontal (untilted) incident X-ray beam, and Q_y is orthogonal to both Q_x and Q_z. The hydrocarbon chains form two-dimensional polycrystals, giving rise to a diffraction pattern that depends on the modulus of the of the in-plane momentum transfer $Q_{xy} = (Q_x^2 + Q_y^2)^{1/2}$ and is practically independent of the sample rotation over the z-axis. We define $Q = (Q_{xy}^2 + Q_z^2)^{1/2}$ as the total momentum transfer.
(39) Kjaer, K. *Physica B* **1994**, *198*, 100.

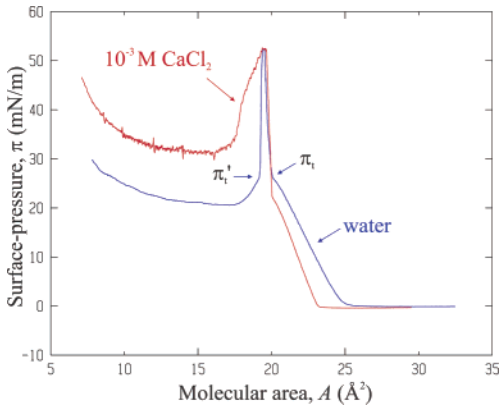

Figure 2. Pressure versus molecular area of AA on H_2O and on a 10^{-3} M $CaCl_2$ solution. The addition of Ca^{2+} to the solution lowers the critical surface pressure (π_t) of the tilted−untilted transition and also removes the transition right after the peak in pressure.

π_t, from untilted to tilted acyl chains. The tilted−untilted transition at π_t depends on chain length and temperature (for arachidic acid at RT, $\pi_t \approx 25.6$ mN/m).[1,4−6,8] The induced collapse of the monolayer, although considered a chaotic process, is to a large extent reproducible. As shown, the fall off in surface pressure from the condensed solid phase is almost a mirror image of the compression part with a transition at π'_t (see Figure 2). Such collapse behavior is characteristic of other fatty acids (stearic acid, behenic acid, and others).[2,11]

The spreading of AA on a Ca^{2+} solution affects the isotherm of the monolayer both before and after the collapse. Figure 2 shows the isotherm of AA on a 10^{-3} M $CaCl_2$ solution before and after collapse. The chain tilted−untilted transition for AA on a Ca^{2+} solution occurs at a lower pressure: $\pi_t \approx 19$ mN/m compared to $\pi_t = 25.6$ mN/m for AA on pure water.

B. Collapse of Arachidic Acid on Pure Water. X-ray reflectivity measurements of AA on water and on solutions were conducted at various pressures before and after collapse. Figure 3A shows the reflectivity curves normalized to the reflectivity of an ideally flat water surface (R/R_F) of AA on water at $\pi \approx$ 20 mN/m and after collapse (molecular area $\sim A_0/2$, $\pi \approx 20$ mN/m). The solid lines are calculated from the corresponding EDs shown in Figure 3C. Table 1gives the adjustable parameters that generate the ED profiles from eq 1, as shown in Figure 3C. The ED of the monolayer on water is in good agreement with that obtained by Kjaer et al. at corresponding surface pressures.[4]

The normalized reflectivity for the collapsed monolayer ($A \lesssim$ 10 Å^2) is significantly different from that of the monolayer before collapse, and it exhibits rather reproducible features, i.e., the minima and the maxima are at the same momentum transfer (Q_z) and differ slightly in intensity for different collapsed samples. These differences are due to inhomogeneities in the collapsed film, which, as shown below by GIXD, consists mainly of trilayers in coexistence with a small amount of monolayers. The calculated ED profile of the collapsed film has an average thickness $d_{total} \approx 75$ Å compared to $d_s \sim 85$ Å, the total thickness of three stretched AA layers (see Table 1). The carboxylic headgroup at the water interface and the two carboxylic groups joining the bilayer at the gas interface give rise to the two maxima in the ED shown in Figure 3C. A schematic layout of the trilayer film is also shown in Figure 3C. This smaller film thickness is due to the fact that the chains are tilted with respect to the surface normal by $\cos^{-1}(d_{total}/d_s) \approx 28°$, consistent with the GIXD results discussed below.

Neutron reflectivities of deuterated AA films before and after collapse on water (H_2O) are shown in Figure 3B. The neutron measurements can be obtained to a maximum momentum transfer, $Q_z \approx 0.23$ Å^{-1}, limiting the spatial resolution of the SLD to

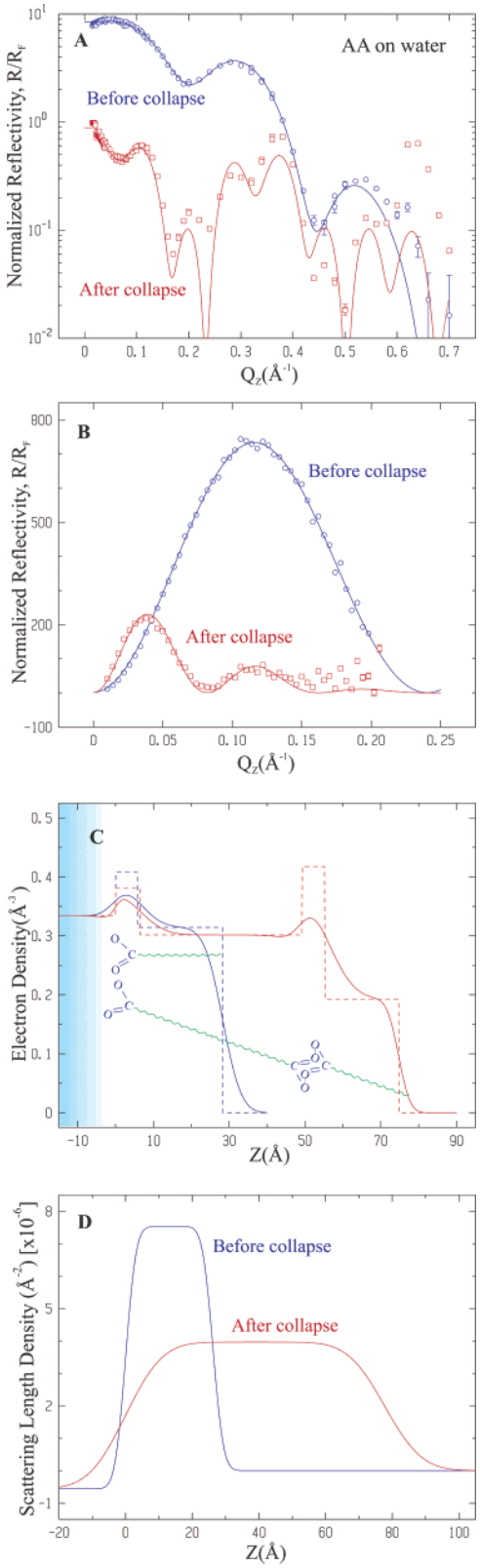

Figure 3. (A) Normalized XRs and (B) NRs of AA on pure H_2O before (circles) and after collapse (squares; XRs are shifted by a decade for clarity). The NRs were conducted on deuterated AA monolayers on H_2O. The solid lines are the calculated reflectivities obtained from a NLSF using the EDs and SLDs shown in (C) and (D), respectively. (C) EDs and (D) SLDs used for fitting the corresponding reflectivity curves in (A) and (B). The dashed lines show the EDs in the absence of interfacial surface roughnesses.

Table 1. Parameters That Generate the Best-Fit Calculated Reflectivities to the Experimental Data for AA on Pure Water before and after Collapse[a]

	before	after
	X-ray Reflectivity	
σ_0 (Å)	3.1 ± 1.0	1.5 ± 1.0
d_{head1} (Å)	5.8 ± 2.0	6.5 ± 1.1
ρ_{head1} (e/Å^3)	0.408 ± 0.027	0.381 ± 0.015
σ_1 (Å)	4.9 ± 0.5	5.3 ± 0.5
d_{chain2} (Å)	22.5 ± 1.6	42.8 ± 1.2
ρ_{chain2} (e/Å^3)	0.314 ± 0.002	0.301 ± 0.003
σ_2 (Å)	3.9 ± 0.3	3.0 ± 0.5
d_{head3} (Å)		5.9 ± 1.2
ρ_{head3} (e/Å^3)		0.418 ± 0.012
σ_3 (Å)		6.0 ± 0.5
d_{chain4} (Å)		19.5 ± 1.4
ρ_{chain4} (e/Å^3)		0.192 ± 0.002
σ_4 (Å)		2.4 ± 0.3
	Neutron Reflectivity	
σ (Å)	2.5 ± 0.7	8.8 ± 1.0
d_{head1} (Å)	26.2 ± 0.5	77.8 ± 2.0
ρ_{head1} ($\times 10^{-6}$ Å^{-2})	7.53 ± 0.21	3.97 ± 0.25

[a] Two- and four-slab models for the monolayer and the trilayer, respectively, are used to generate the ED profiles shown in Figure 3C. A single-slab model SLD (Figure 3D) is used to fit the NRs of the films before and after collapse with a single surface roughness for all interfaces.

practically a single slab (assigning a distinct SLD to the headgroup region and the chain overparametrizes the model; i.e., one SLD box is sufficient to obtain an adequate fit). The model SLDs for the monolayer and the collapsed film are shown in Figure 3D. The total thickness of the monolayer before collapse is 26.2 Å, and it is 77.8 Å after collapse, consistent with the X-ray reflectivity analysis (Table 1). Neutron reflectivities from the deuterated monolayer before and after collapse on D_2O as a subphase were also measured and analyzed. Although the analysis of the data is consistent with the results mentioned above, the SLD contrast between the film and the subphase is not strong and the signal due to the film is weak.

GIXD patterns from AA monolayers on water before and after collapse versus in-plane momentum transfer ($Q_{xy} \equiv (Q_x^2 + Q_y^2)^{1/2}$) integrated over Q_z range from 0.0 to ~0.2 Å^{-1} are shown in Figure 4A. Before collapse (at 20 mN/m), we find that the diffraction pattern is relatively simple, consistent with previous reports.[8] The analysis of the Bragg reflections and the rod scans show orthorhombic packing of the hydrocarbon chains in the so-called herringbone (HB) structure. The lattice constants of the orthorhombic structure associated with these peaks are a_S = 4.8 Å and b_S = 8.1 Å. The projection of the chain's subcell onto a plane perpendicular to the chain's long axis is orthorhombic, denoted as the $O_\perp$ structure for acyl chains,[40] as shown in Figure 4D. Analysis of the rod scans using eq 3 yields an average chain tilt angle with respect to the surface normal (15 ± 3°) with a chain tilt toward the nearest neighbors (NNs).

The diffraction for the collapsed film ($\pi \approx 20$ mN/m) is more complicated due to the presence of minute multiple phases. However, the diffraction pattern exhibits two very strong peaks, one at Q_{xy} = 1.405 and Q_z = 0.614 Å^{-1} (Q = 1.5342 Å^{-1}; ref 38) and the second at Q_{xy} = 1.698 and Q_z = 0.0 Å^{-1}, due to the majority phase. These two peaks, labeled (1,1) and (0,2), respectively, are defined in the in-plane subcell of the acyl chains, which is tilted with respect to the surface. The two reflections correspond to the subcell lattice constants, a_S = 4.918 Å and b_S

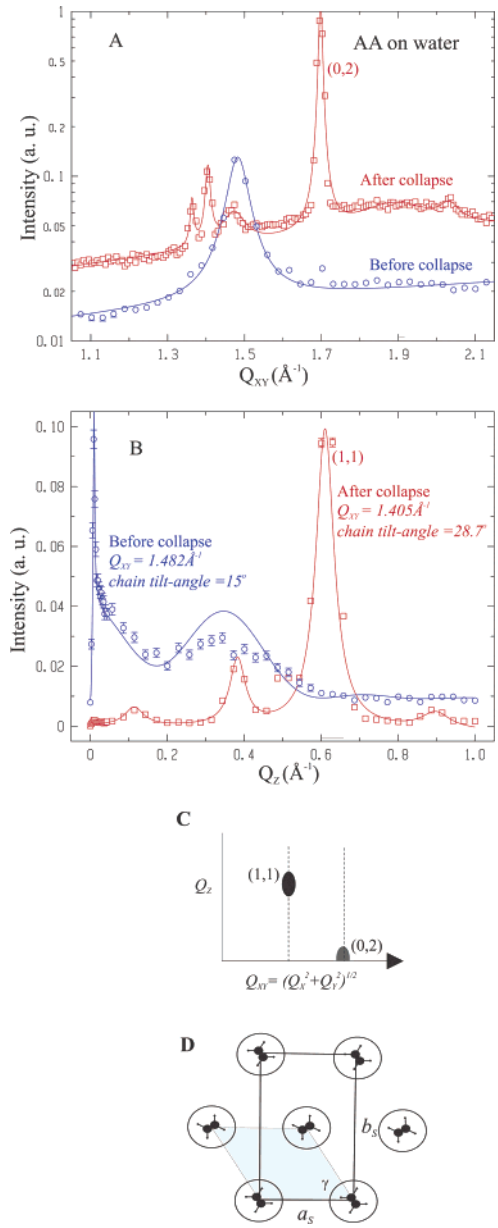

Figure 4. (A) GIXD scans of AA monolayers on H_2O before (circles) and after collapse (squares) versus in-plane momentum transfer ($Q_{xy} \equiv (Q_x^2 + Q_y^2)^{1/2}$ integrated over a Q_z range from 0.0 to ~0.2 Å^{-1}). (B) Rod scans from the prominent Bragg reflections as indicated before (circles) and after collapse (squares). (C) Schematic illustration of the two main reflections observed in the (Q_{xy}, Q_z) plane. (D) Projection of a subcell of the hydrocarbon chains onto a plane perpendicular to the chain long axis (herringbone, $O_\perp$ packing).

= 7.400 Å, with a chain cross section of 18.2 Å^2. The average tilt angle of the chains from the surface normal can be readily calculated by

$$\tan t = \frac{Q_z(1,1)}{(Q_{xy}(1,1)^2 - (Q_{xy}(0,2)/2)^2)^{1/2}} \qquad (5)$$

with t = 28.7°, where each chain is tilted toward its NN. The lattice parameters and tilt angles of the chains are practically the same as those found in the single crystals of a few fatty acids,[40,41] where it is found that a_S = 4.92 Å and b_S = 7.40 Å. We performed GIXD measurements on collapsed films at densities (nominal

(40) Larsson, K. *Lipids—Molecular Organization, Physical Functions and Technical Applications*; The Oily Press Ltd.: Dundee, Scotland, 1994.

(41) von Sydow, E. *Acta Crystallogr.* **1955**, *8*, 557.

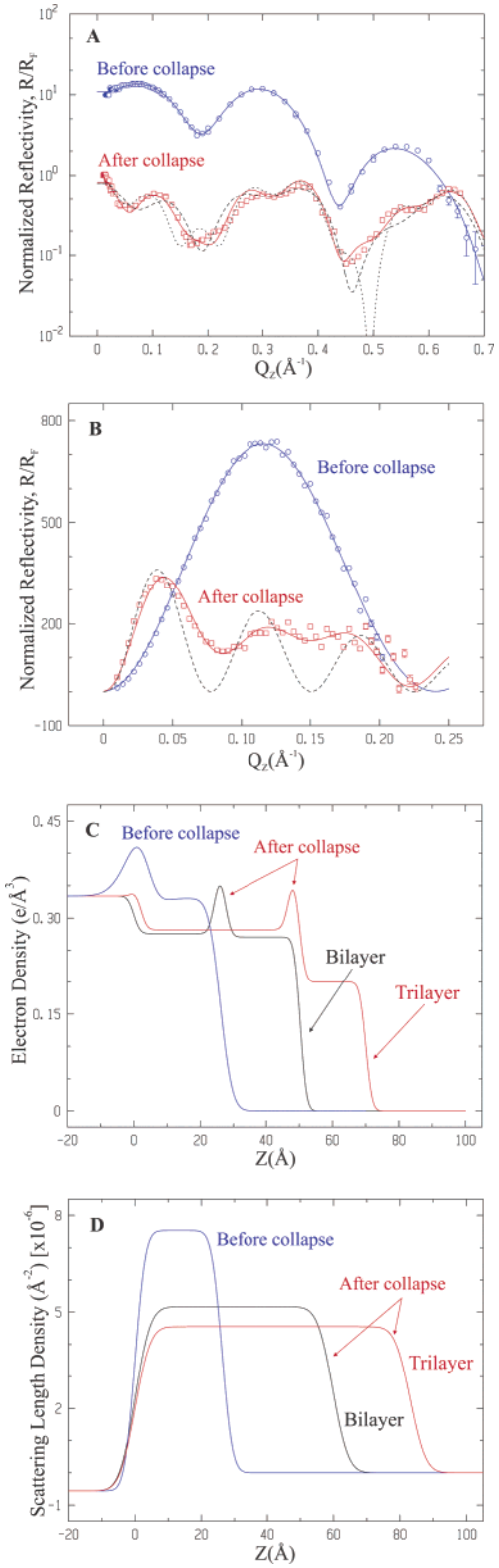

Figure 5. (A) Normalized XRs and (B) NRs of AA on a 10^{-3} M $CaCl_2$ solution before (circles) and after collapse (squares). The collapsed film was obtained by continuous compression of the monolayer after spreading, without aging the monolayer. The solid lines are the best-fit curves as discussed in the text, and the dashed and dotted lines are the best-fit curves assuming 100% bilayer and 100% trilayer structures, respectively. (C) EDs and (D) SLDs of the bi- and trilayers used for the best-fit curves (solid lines) in (A). The dashed line in (B) is the best fit assuming a trilayer structure (fixed thickness at ∼80 Å).

molecular areas) that enable the formation of a trilayer film, as evidenced in our analysis of reflectivity. It is, therefore, remarkable that a trilayer film on the surface of water exhibits an in-plane crystalline quality that is comparable to that of 3D crystals.

Although the collapse produces primarily the HB phase, it is well-known that fatty acids display diverse polymorphism when they are crystallized.[42] It is, therefore, not surprising that the GIXD pattern shows other, although weaker, peaks due to minority phases. One such phase is that of the monolayer before collapse, as we find Bragg reflections that coincide with those of the monolayer prior to collapse. The observed reflections at Q_{xy} = 1.364, 1.473, and 1.405 Å^{-1} can be attributed to an oblique unit cell with lattice constants of a_S = 5.365 Å, b_S = 4.967 Å, and γ = 59.2° (molecular area, 22.88 Å^2).

C. Collapse of Arachidic Acid on a $CaCl_2$ Solution. The collapse of arachidic acid on a Ca^{2+} solution depends on the compression protocol, as mentioned above. In the first protocol, the monolayer is compressed continuously to a nominal molecular area, A, that is smaller than the chain cross section, $A_0/3 \lesssim A \lesssim A_0/2$, i.e., *collapse by continuous compression*. And in the second protocol, the monolayer is *aged* by compressing it to molecular areas larger than A_0 at finite pressures and allowing it to equilibrate for 6−12 h and then compressing it to collapse, i.e., *aged film*.

C.1. Collapse by Continuous Compression. Figure 5A shows the normalized reflectivities of AA on a 10^{-3} M $CaCl_2$ solution before collapse and after compressing the film continuously to collapse. The reflectivity of the monolayer on a Ca^{2+} solution is similar to that of AA on pure water, but overall, it is more intense. Qualitatively, this is evidence for an increase in the electron density in the monolayer due to the formation of a bound Stern layer of Ca^{2+} ions at the carboxylic headgroup. The best-fit calculated reflectivity is obtained by the NLSF of the model ED shown in Figure 5C and in Figure 6B. In Table 2, the parameters used to fit the reflectivity data are listed. The integrated ED of the headgroup region is significantly larger than that obtained for AA on pure water. A more detailed analysis, applying space-filling constraints and volume constraints,[34,35,43,44] yields 0.31 ± 0.1 Ca^{2+} ions per AA molecule and 1.5 ± 0.5 water molecules in the headgroup region. The number of ions per molecule differs slightly from that found in similar studies of AA spread on divalent ions in solution,[45] but it is in agreement with the results from the infrared absorption spectroscopy studies of AA acid spread on a Ca^{2+} solution.[46]

The best fit to the XR of the collapsed monolayer shown by the solid lines in Figure 5A required the use of eq 2 and the parameters of a mixed film consisting of 38.4% bilayer and 61.6% trilayer with EDs as shown in Figure 5C. A similar fit to the NRs shows the film consists of 7.5% monolayer, 42.0% bilayer, and 50.5% trilayer. The parameters used to calculate the best-fit reflectivities are listed in Table 2. As mentioned earlier, our NR is not sensitive to the difference in the SLD between the headgroup and the chain. It only indicates that there are two main film components (domains) with different thicknesses. Thus, according to the NR, the SLD associated with the bilayer can be due to either an inverted or a noninverted bilayer (i.e., headgroup exposed to the gas phase). We have, therefore, attempted to fit the X-ray data with a mixture that includes the noninverted bilayer. Although this model produces the features of the normalized reflectivity, it yields an inferior fit compared to that obtained with the inverted bilayer model. For comparison,

(42) Kaneko, F.; Sakashita, H.; Kobayashi, M.; Kitagawa, Y.;Matsuura, Y.; Suzuki, M. *Acta Crystallogr. C* **1994**, *50*, 245.
(43) Gregory, B. W.; Vaknin, D.; Gray, J. D.; Ocko, B. M.; Stroeve, P.; Cotton, T. M.; Struve, W. S. *J. Phys. Chem. B* **1997**, *101*, 2006.
(44) Vaknin, D.; Kelley, M. S. *Biophys. J.* **2000**, *79*, 2616.
(45) Bloch, J. M.; Yun, W. *Phys. Rev. A* **1990**, *41*, 844.
(46) Le Calvez, E.; Blaudez, D.; Buffeteau, T.; Desbat, B. *Langmuir* **2001**, *17*, 670.

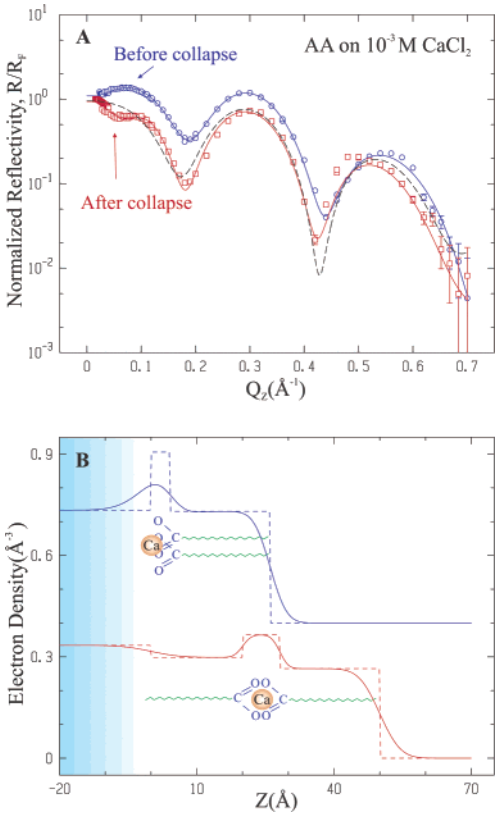

Figure 6. (A) Normalized XRs of AA on a 10^{-3} M $CaCl_2$ solution before (circles) and after collapse (squares). The collapsed film was formed by compressing an *aged* monolayer on which several X-ray studies were performed. The solid lines correspond to the best calculated fit as discussed in the text. The dashed line is the best attempted fit assuming a monolayer-like film with a two-slab ED model. (B) EDs used for fitting the reflectivity curves in (A). The ED for the monolayer before collapse is shifted by 0.4 e/Å^3 for clarity. After collapse, an inverted bilayer of calcium di-arachidate is formed on the solution with the hydrocarbon chains in contact with the water.

we also include the best-fit data assuming 100% bilayer (dashed line) and 100% trilayer (dotted line). The ED of the bilayer structure is consistent with the formation of an elongated AA dimer, as discussed in more detail below.

C.2. Collapse after Aging the Monolayer. Figure 6 shows the XR of the monolayer before (circles) and after (square) collapse on a 10^{-3} M $CaCl_2$ solution. The collapsed film was obtained after measuring the reflectivities and GIXDs from the monolayer at a finite pressure (this takes 8−16 h), namely after aging the monolayer. The normalized reflectivity from the collapsed monolayer ($\pi = 35$ mN/m), although surprisingly similar to the reflectivity before collapse, has some subtle but reproducible differences. Compared to the reflectivity of the monolayer before collapse, the reflectivity after the collapse has lower intensities at small Q_z values; it has a minimum at $Q_z \sim 0.05$ Å^{-1}, and the other minima are slightly shifted to smaller Q_z values. The ED profile that produces the best fit to the measured reflectivity is shown in Figure 6B, and the parameters are listed in Table 3. The film has a total thickness $d_{total} \approx 50$ Å, significantly smaller than the thickness observed for the collapsed monolayer on pure water ($d_{total} = 75$ Å). It is also significantly larger than the thickness of a single layer. This is clearly due to the formation of a bilayer at the interface, the details of which we determined by the space filling analysis. The detailed ED profile of the collapsed monolayer on a Ca^{2+} solution exhibits three slabs of distinct EDs. The first slab at the water interface and at the air interface is associated with acyl chains that, in general, have EDs in the range 0.29−0.33 e/Å^3. The intervening layer (thickness, ∼8 Å) is associated with two carboxylic headgroups that are bound together by a Ca^{2+} ion including a water molecule forming a calcium oxalate monohydrate intercalated between two acyl chains. Although the 100% inverted bilayer structure could be consistently reproduced at the synchrotron and on an in-house reflectometer, it was not obtained *in situ* with the neutron reflectivity experiments. This may be due to different sample preparation conditions that we have not been able to determine. Another possibility is that the X-rays create radicals, such as H_2O_2, and ionize the headgroup even under the inert environment surrounding of the monolayer, i.e., helium, inducing the formation of a bilayer structure. We emphasize that our results are not conclusive with regard to the inverted bilayer, and they require more corroborating evidence, which we are pursuing at this time

GIXD patterns from the AA monolayers on a 10^{-3} M $CaCl_2$ solution before and after collapse versus in-plane momentum transfer are shown in Figure 7A. The GIXD from the monolayer

Table 2. Parameters That Produce the Best-Fit Calculated Reflectivities to the Experimental Data for AA on a 10^{-3} M $CaCl_2$ Solution before and after Collapse[a]

X-ray Reflectivity Parameters			
	before	after	
	monolayer	38.4% bilayer	61.6% trilayer
σ_0 (Å)	5.3 ± 1.2	1.5 ± 0.4	1.5 ± 0.4
d_{head1} (Å)	4.0 ± 2.7		2.0 ± 0.5
ρ_{head1} (e/Å^3)	0.511 ± 0.070		0.350 ± 0.060
σ_1 (Å)	2.8 ± 0.5		1.5 ± 0.4
d_{chain2} (Å)	22.0 ± 0.5	24.4 ± 0.6	45.0 ± 0.5
ρ_{chain2} (e/Å^3)	0.332 ± 0.002	0.276 ± 0.004	0.282 ± 0.036
σ_2 (Å)	2.8 ± 0.3	1.5 ± 0.4	1.5 ± 0.4
d_{head3} (Å)		3.0 ± 1.0	3.0 ± 0.2
ρ_{head3} (e/Å^3)		0.385 ± 0.013	0.386 ± 0.013
σ_3 (Å)		1.5 ± 0.4	1.5 ± 1.0
d_{chain4} (Å)		22.9 ± 0.5	20.1 ± 1.0
ρ_{chain4} (e/Å^3)		0.270 ± 0.030	0.20 ± 0.023
σ_4 (Å)		1.5 ± 0.4	1.5 ± 1.0
Neutron Reflectivity Parameters			
	before	after	
	monolayer	42.0% bilayer	50.5% trilayer
σ (Å)	2.5 ± 0.4	3.7 ± 1.2	3.7 ± 1.3
d_1 (Å)	26.2 ± 0.5	59.8 ± 3.0	83.1 ± 2.0
ρ_1 ($\times 10^{-6}$ Å^{-2})	7.53 ± 0.10	5.17 ± 0.10	4.55 ± 0.25

[a] The two-slab model is used for the monolayer, whereas the three- and four-slab models are used to represent the bi- and trilayer mixtures after collapse. The same parameters are also used to show the EDs and SLDs in Figure 5C and D. The NR from the collapsed film contains 7.5% monolayer with the same parameters as those shown in the column for the monolayer.

Table 3. Parameters Used to Calculate the Best-Fit Reflectivities to the Measurements of Collapsed AA on 10^{-3} M $CaCl_2$ after Aging (Figure 6A)[a]

σ_0	10.0 ± 2.8
d_{chain1}	20.0 ± 0.5
ρ_{chain1} (e/Å^3)	0.298 ± 0.002
σ_1	1.5 ± 0.1
d_{head1} (Å)	8.1 ± 0.8
ρ_{head1} (e/Å^3)	0.365 ± 0.02
σ_2	1.5 ± 0.1
d_{chain2} (Å)	21.8 ± 0.4
ρ_{chain2} (e/Å^3)	0.266 ± 0.003
σ_3	3.6 ± 0.5

[a] These parameters generate the EDs shown in Figure 6B using eq 1.

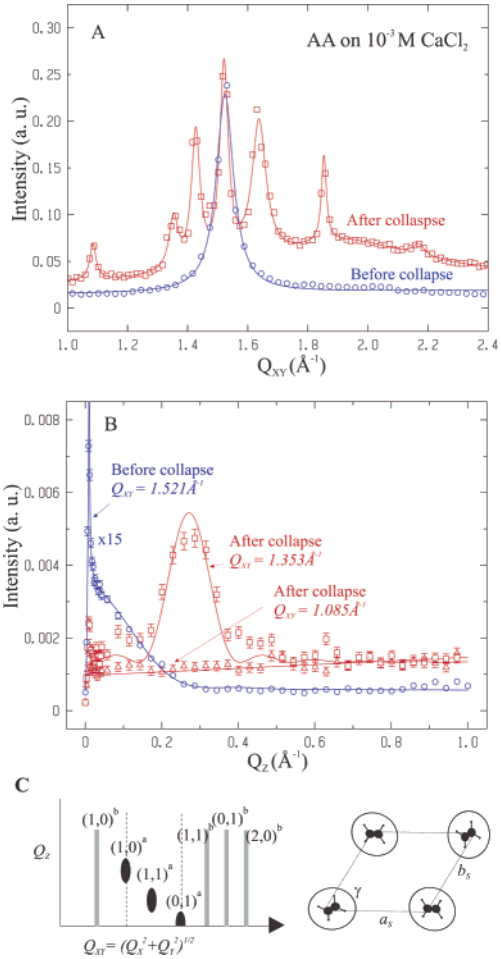

Figure 7. (A) GIXD scans of AA on a 10^{-3} M $CaCl_2$ solution before (circles) and after collapse (squares) on an *aged* film. Before collapse, a single Bragg peak due to the ordering of the acyl chains is observed. (B) Rod scans through prominent Bragg reflections before (circles) and after collapse (squares and triangles) as indicated. (C) Schematic illustration of the Bragg reflections after collapse observed in the (Q_{xy}, Q_z) plane. Two sets of peaks distinguished by their rod scans are observed: the rodlike scans are due to the headgroup ordering (calcium oxalate formation), and the peaked ones are due to the ordering of the elongated di-arachidate molecule dominated by chain ordering.

has a single Bragg reflection at $Q_{xy} = 1.521$ Å^{-1} and at $Q_z = 0$ Å. A rod scan through this peak, shown in Figure 7B, establishes that the hydrocarbon chains are hexagonally packed with a tilt angle of $t \lesssim 4°$ with respect to the surface normal. The lattice constant of the hexagonally ordered chains is $a = 4.77$ Å, with a corresponding molecular area of $A = 19.7$ Å^2.

The GIXD data and rod scans of the collapsed monolayer confirm the formation of an inverted bilayer of calcium di-arachidate. The diffraction pattern consists of two sets of Bragg reflections (shown in Figure 7A and B): one associated with the ordering of the long acyl chains and the other associated with the crystallinity of calcium oxalate. The two sets are distinguished by their rod scans, as depicted in Figure 7C. Whereas the 2D crystals of calcium oxalate practically exhibit constant-intensity rod scans, characteristic of a 2D system, the rod scans from peaks associated with the chains show distinct maxima at finite Q_z values. Figure 7B shows two rod scans: one associated with the chains and the other associated with a single layer of calcium oxalate. Detailed analyses of the rod scans yielded a molecular tilt angle of ~12.6° from the surface normal. The line width of the peak (denoted (1,0)), $\Delta Q_z \approx 0.12$ Å^{-1}, is inversely proportional to the thickness of the ordered film, $d_{total} = 2\pi/\Delta Q_z \approx 52.4$ Å. This is in excellent agreement with the ~50 Å film thickness extracted from the reflectivity above. The peak positions and indices of the Bragg peaks are given in Table 4. The three fundamental nondegenerate Bragg peaks associated with the chain ordering indicate that the unit subcell is oblique, as depicted in Figure 7C, with the lattice parameters $a_S = 5.304$ Å and $b_S = 4.809$ Å and an angle $\gamma = 59.2°$. The other four peaks due to the headgroup ordering (i.e., calcium oxalate monohydrate) can be indexed on a different in-plane unit cell: $a_{CaO} = 6.603$ Å, $b_{CaO} = 3.864$ Å, and $\gamma = 61.3°$. The molecular areas of the sublattice unit cells of the chains and of the calcium oxalate headgroups are 21.91 and 22.38 Å^2, respectively. These two substructures belong to a larger unit cell that we have not been able to determine uniquely. Our analysis points to a minimum unit cell consisting of $5a_S \times 4b_S$ with a slight rotation, but larger unit cells are also possible.

Table 4. Best-Fit Parameters to the Diffraction Scans of AA on 10^{-3} M $CaCl_2$ after Collapse by Aging[c]

peak	Q_{xy} (Å^{-1})	Δ (Å^{-1})	intensity (au)
(1,0)[a]	1.353 ± 0.004	0.018	0.056
(1,1)[a]	1.427 ± 0.009	0.017	0.144
(0,1)[a]	1.521 ± 0.001	0.017	0.212
(1,0)[b]	1.085 ± 0.006	0.013	0.039
(1,1)[b]	1.638 ± 0.005	0.029	0.148
(0,1)[b]	1.854 ± 0.001	0.010	0.092
(2,0)[b]	2.169 ± 0.003	0.024	0.013

[a] Indexing according to the oblique chain unit subcell yields ($a_S = 5.304$ Å, $b_S = 4.809$ Å, $\gamma = 59.2°$). [b] Indexing according to the calcium oxalate subcell yields ($a_{CaO} = 6.603$ Å, $b_{CaO} = 3.864$ Å, $\gamma = 61.3°$). [c] Nominal molecular area, ≈11 Å^2

IV. Discussion

The isotherms in Figure 2 show that the maximum surface pressure the 2D film can withstand is approximately $\pi \sim 55$ mN/m, occurring at the close-packed area of the hydrocarbon chains, in agreement with other studies,[2,47] but it is practically independent of salt concentration. This may suggest that the initial collapse point (ICP) is a property related to the topological defects of the closely packed hydrocarbon chains. The most obvious candidate defects are the grain boundaries separating the different crystallites. Based on our experience, the ICP and maximum achievable pressure depend on the cleanliness of the water surface, the purity of the molecules constituting the monolayer, and the compression rate, but the pressure does not exceed ~55 mN/m. Beyond the ICP, the isotherms (Figure 2) show that the collapse proceeds differently depending on the ionic content of the subphase.

The structural studies presented here demonstrate that induced collapse may be described by the balance of intermolecular forces.[55] It is, therefore, important to understand the state of the monolayer and the subphase before collapse. First, we estimate the surface charge density of AA on pure water at a roughly

(47) Valdes-Covarrubias, M. A.; Cadena-Nava, R. D.;Vasquez-Martinez, E.; Valdez-Perez, D.; Ruiz-Garcia, J. *J. Phys.: Condens. Matter* **2004**, *16*, S2097.
(48) Ninham, B. W.; Parsegian, V. A. *J. Theor. Biol.* **1971**, *31*, 405.
(49) Israelachvili, J. N. *Intermolecular and Surface Forces*; Academic Press: London, U.K., 2000.
(50) Bu, W.; Vaknin, D.; Travesset, A. *Phys. Rev. E* **2005**, *72*, 060501; *Langmuir* **2006**, *22*, 5673.
(51) Travesset, A.; Vaknin, D. *Europhys. Lett.* **2006**, *74*, 181.
(52) Tanford, C. *The Hydrophobic Effect: Formation of Micelles and Biological Membranes*; John Wiley & Sons: New York, 1980.
(53) Jeffrey, G. A. *An Introduction to Hydrogen Bonding, Topics in Physical Chemistry*; Oxford University Press: New York, 1997.
(54) McConnell, H. M.; Moy, V. T. *J. Phys. Chem.* **1988**, *92*, 4520.
(55) Lorenz, C. D.; Travesset, A. *Langmuir* **2006**, *22*, 10016.

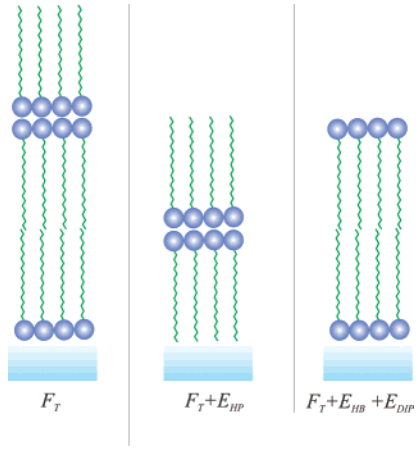

Figure 8. Sketch of possible stacking of fatty acids resulting from the induced collapse of their Langmuir monolayer. The trilayer model (A) has the lowest free energy, F_T, whereas the other models are higher in energy by the hydrophobic effect (E_{HP}, model B) and by noncanceling electric dipole−dipole interactions and uncompensated hydrogen bonding ($E_{HP} + E_{DIP}$, model C).

neutral pH (usually, the pH of water is slightly below 7 due to the dissolution of CO_2 from air). The Debye screening length in pure water is $\lambda_D \approx 10^4$ Å. Using the renormalized surface charge Poisson−Boltzmann theory (RPB)[48−50] and a p$K_a \approx 5.1$ for the carboxylic headgroup, we estimate that less than ∼0.5% of all AA molecules release their proton and become charged;[49,51] i.e., the surface is practically neutral at pH ∼ 7. Therefore, interactions in the monolayer are dominated by hydrogen bonding and dipolar interactions. These interactions are similar in strength to the interactions among water molecules.

Figure 8 shows a sketch of three possible structures that can arise from an induced collapse of AA on water. The free energies of configurations B and C are higher than that of structure A. In structure B, the free energy is higher due to the hydrophobic effect arising from the acyl chain−water contact. The cost in free energy per chain for such a contact is comparable to the energy required to dissolve a methane molecule in water, $\sim 6k_BT$ (ref 52, this estimate is not much different if the long wavelength hydrophobic effect is used instead). Structure C has a headgroup exposed to air that is in contact with water before the collapse and, therefore, suffers a loss of one hydrogen bond per molecule, resulting in excess free energy ($\sim 6k_BT$ per molecule).[53] In addition, there is an unfavorable energy cost from the alignment of the electric dipole moments of the headgroups.[54] Furthermore, if structure C is formed, the system would show a strong tendency to dissolve in solution, and given the large length of the hydrocarbon chains, small micelles are not possible. It should be noted that configuration A is favored only by a few k_BT units over B and C and other possible configurations. A more detailed discussion on the formation of these structures is provided elsewhere.[55]

The conditions of the AA monolayers on $CaCl_2$ solutions are somewhat different than those in pure water. First, the surface charge of the monolayer in the presence of Ca^{2+} is substantial, as most AA headgroups are charged, a result confirmed both from the present study and from other reports.[4,46] From the isotherm in Figure 2, it is apparent that significant surface pressure is needed for the collapse to proceed, which can be estimated as $\pi A_0 \sim 3k_BT$ per AA chain, where $\pi = 40$ mN/m. Figure 9 depicts the two *a priori* most favorable configurations of the folded AA monolayer on a $CaCl_2$ solution. The structure formed (whether A or B) depends on the competition between the cohesive electrostatic energy and the hydrophobic interactions and other

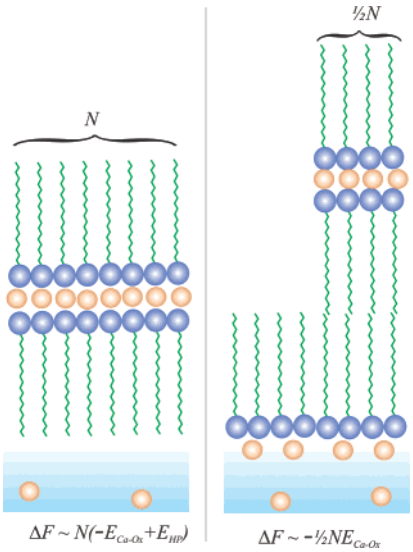

Figure 9. Schematic illustration of two possible models for the stacking of fatty acids resulting from the induced collapse of their Langmuir monolayer on a $CaCl_2$ solution. The favorable binding energy for forming a calcium oxalate is much lower than that for any of the other interactions; the configuration with the maximum number of oxalates will be favored. This explains why configuration A, which exploits all *N*-squeezed molecules to form *N* calcium oxalates, is favored over configuration B, for which the number of calcium oxalates formed is only *N*/2.

factors.[55] If the electrostatic cohesive energy is dominant, the configuration with the maximum number of calcium di-arachidate molecules formed from *N*-ejected molecules is favored. As depicted in Figure 9, twice as many calcium di-arachidate pairs are formed from *N*-ejected amphiphiles in configuration A, compared to *N*/2 in configuration B, thus favoring the bilayer structure. If the hydrophobic cost (of the order of $6k_BT$ per chain) dominates over the cohesive electrostatic energy, the trilayer is favored. As discussed more extensively in ref 55, this balance of free energies is subtle and is further complicated by the long relaxation times of the system, which makes the exact ratio of bilayer to trilayer difficult to predict. In either case, it is clear that the collapsed phase is favored over a monolayer kept at constant pressure. The fact that the inverted bilayer is not observed in a spontaneous collapse may be due to an activation barrier, arising from the work needed to eject an AA molecule together with a calcium ion while inverting a given AA molecule. We estimate this work as $\pi A_0 \sim 3k_BT$ per AA chain, where $\pi = 40$ mN/m and is a typical surface pressure (as it follows from the isotherm in Figure 2). It seems, therefore, plausible that, after long relaxation times, the structures observed by induced collapse may be observed spontaneously.

The collapse of AA monolayers on $CaCl_2$ solutions produces an unusual but stable double-layer arachidate phase at the interface, with the methyl group of the chain in contact with the water interface. This is similar to the spreading of long chain alkanes at the interface. Recent X-ray studies revealed that long chain alkanes (longer than C36) form stable monolayers at the air/water interface,[56] and therefore the formation of the inverted bilayer (structure A) is not as surprising as it seems.

V. Conclusions

Using neutron and X-ray scattering studies, we determined the structures of AA films before and after collapse on pure

(56) Weinbach, S. P.; Weissbuch, I.; Kjaer, K.; Bauwman, W. G.; Als-Nielsen, J.; Lahav, M.; Leiserowitz, L. *Adv. Mater.* **1995**, *7*, 857.

water and on Ca^{2+} solutions. AA on pure water collapses by forming primarily a trilayer structure, as shown in Figure 8A. Although this trilayer structure has been proposed by studies carried out on films transferred to a solid support, we provide, to our knowledge, the first *in situ* experimental evidence for this structure. For AA spread on the divalent ion Ca^{2+}, we found structures consisting of inverted bilayer and trilayer mixtures, whose final composition depends on the compression protocol. This clearly shows that AA monolayers spread on Ca^{2+} solutions exhibit a wide range of extremely slow relaxation times, which essentially prevent the system from reaching thermal equilibrium. Rather surprisingly, with a certain compression protocol it is possible to obtain a pure inverted bilayer with no appreciable trilayer fraction. It should be noted that we cannot exclude X-ray radiation modification of the film as the cause for the appearance of this pure bilayer phase, as it was not observed in the neutron reflectivity measurements. The hydrocarbon chains of the stretched pairs are crystalline with an oblique subcell packing structure, whereas the intercalated calcium induces the crystallinity of calcium oxalate monohydrate ($COO-Ca-OOC-H_2O$).

We discussed the different possible structures that can be formed by collapse (a detailed discussion can be found in ref 55). We also estimated that the activation energy separating these two states is $3k_BT$ per chain, suggesting that the collapsed structure can be obtained spontaneously. It is, therefore, likely that the crystallites observed during spontaneous collapse reported in ref 13 correspond to the inverted bilayers found in the present study.

Our results are significant to recent experiments on the dewetting of water near hydrophobic surfaces, as the inverted bilayer presents a hydrophobic surface in contact with water. Recent neutron scattering experiments[57−59] provide evidence of a thick depletion zone (of the order of 10 Å) of water vapor between the hydrophobic surface and the water. On the other hand, X-ray experiments[60] on very long chains (containing 36 hydrocarbon groups[56]) find a much smaller depletion zone, of the order of 1 Å. Also, neutron reflectivity studies of the polystyrene/water interface found that the intrinsic depletion layer between the hydrophobic interface (polystyrene) and the water either is negligible or does not exist at all.[61] Although our experiments have not been designed to investigate the problem of water near a hydrophobic interface, our model structure for the inverted bilayer is only compatible with a depletion zone of the order of less than 1 Å.

There are a number of remaining unresolved questions that will require further investigations, such as how the collapsed structures vary for other divalent ions, such as cadmium and barium, or trivalent ions, such as lanthanum, or how the collapse regime may change for molecules with longer chains. We hope that further experimental and theoretical work will clarify these issues.

Acknowledgment. We thank S. Dahlke for assistance with sample preparation and preliminary analysis and D. S. Robinson and D. Wermeille for technical support at the 6-ID beamline. The Midwest Universities Collaborative Access Team (MUCAT) sector at the APS is supported by the U.S. Department of Energy, Basic Energy Sciences, through the Ames Laboratory under Contract No. W-7405-Eng-82. Use of the Advanced Photon Source was supported by the U.S. Department of Energy, Basic Energy Services, Office of Science, under Contract No. W-31-109-Eng-38. The work of A.T. has been supported by NSF-DMR-0426597.

LA062672U

(57) Doshi, D. H.; Watkins, E. B.; Israelachvili, J. N.; Majewski, J. *Proc. Nat. Acad. Sci. U.S.A.* **2005**, *102*, 9458.
(58) Steitz, R.; Gutberlet, T.; Hauss, T.; Klosgen, B.; Krastev, R.; Schemmel, S.; Simonsen, A. C.; Findenegg, G. H. *Langmuir* **2003**, *19*, 2409.
(59) Schwendel, T. R.; Hayashi, T.; Dahint, R.; Pertsin, A.; Grunze, M.; Steitz, R.; Schreiber, F. *Langmuir* **2003**, *19*, 2284.
(60) Jensen, T. R.; Jensen, M. O.; Reitzel, N.; Balashev, K.; Peters, G. H.; Kjaer, K.; Bjornholm, T. *Phys. Rev. Lett.* **2003**, *90*, 86101.
(61) Seo, Y.-S.; Satija, S. *Langmuir* **2006**, *22*, 7113.